Acta Materialia 143 (2018) 174–180

Contents lists available at ScienceDirect

Acta Materialia

journal homepage: www.elsevier.com/locate/actamat

Full length article

Oxidation-resistant metallized nanofibers as transparent conducting films and heaters

Seongpil An [a, b, 1], Yong Il Kim [a, 1], Hong Seok Jo [a], Min-Woo Kim [a], Mark T. Swihart [c], Alexander L. Yarin [a, b, **], Sam S. Yoon [a, *]

[a] School of Mechanical Engineering, Korea University, Seoul 02841, Republic of Korea
[b] Department of Mechanical and Industrial Engineering, University of Illinois at Chicago, 842 W. Taylor St., Chicago, IL 60607-7022, USA
[c] Department of Chemical & Biological Engineering, University at Buffalo, The State University of New York, Buffalo, NY 14260-4200, USA

ARTICLE INFO

Article history:
Received 2 June 2017
Received in revised form
29 August 2017
Accepted 30 September 2017
Available online 3 October 2017

Keywords:
Electrospinning
Electroplating
Nickel-electroplated fiber
Core-shell copper/nickel-electroplated fiber
Transparent conducting film
Transparent heater

ABSTRACT

Transparent conducting films (TCFs) and transparent heaters (THs) are of interest for a wide variety of applications, from displays to window defrosters. Here, we demonstrate production of highly flexible, conducting, and transparent nickel (Ni) electrodes suitable for use not only in TCFs and THs but also in some other engineering applications. The merging of fibers at their intersections (i.e. self-junctioning) minimizes contact resistance in these films. The Ni electrodes exhibited a remarkably low sheet resistance of 0.73 Ω sq^{-1} at an optical transmittance of 93%. This low sheet resistance allows them to serve as low-voltage heaters, achieving a heating temperature of 373 °C at an applied voltage of 2 V. The innate corrosion resistance of Ni allows these electrodes to be used in air at temperatures exceeding 200 °C, and it is expected to help the electrodes to find wide use in a range of industrial applications requiring long-term electrode service. Furthermore, we fabricated perfectly core-shell-structured Cu/Ni electrodes, which exhibited both the excellent electrical properties of Cu and the high corrosion resistance of Ni.

1. Introduction

Micro- and nano-structured electrodes have recently attracted significant attention, for use in transparent conducting films (TCFs), transparent heaters (THs), and related applications. TCFs and THs based on various conducting nanomaterials have been recently reported, including graphene [1–5], carbon nanotubes (CNTs) [6–9], and metal nanowires (NWs) [10–18]. The practical application of these films benefits from recent developments in scalable fabrication techniques. The TCFs represent one of the most important components in several electronic devices, such as light-emitting diodes (LEDs) [19,20], touchable displays [3,8], and solar cells [21,22]. On the other hand, the THs can be used in a variety of consumer and industrial applications, from transparent toasters to window defrosters [23].

Indium tin oxide (ITO) has long been the most commonly-used electrode material for both TCFs and THs. However, the need for alternative materials has increased dramatically in recent decades due to the unstable supply of ITO, primarily due to the rising cost of indium. Moreover, the disadvantages of ITO such as its brittleness are recognized as critical drawbacks, limiting its use in the next-generation flexible electronic devices, such as flexible cellphones and bendable batteries. Alternatives to ITO should not only exhibit greater flexibility but should aim to resolve the inevitable trade-off between the low sheet resistance (R_s) and high transmittance (T_r).

Metal NWs have shown very promising performances when used in both TCFs and THs. For instance, sparse metal nanowire films can have a low R_s (lower than 10 Ω sq^{-1}) and can be heated to a high temperature (T) (higher than 200 °C), while exhibiting sufficient T_r for most applications. For example, An et al. [24] recently reported novel copper (Cu)-electroplated wires (CuEWs) that revealed remarkably low R_s values of the order of 10^{-1} Ω sq^{-1}, combined with $T_r > 97\%$. In contrast to this improvement in the performance of TCFs, the heating capability of metal NWs remains limited. Most metal NWs undergo oxidization when heated in air, which increases their resistance (converting conductive metal into less conductive or insulating metal oxide). This reduces the power

* Corresponding author. School of Mechanical Engineering, Korea University, Seoul 02841, Republic of Korea.
** Corresponding author. Department of Mechanical and Industrial Engineering, University of Illinois at Chicago, Chicago 60607-7022, USA.
E-mail addresses: ayarin@uic.edu (A.L. Yarin), skyoon@korea.ac.kr (S.S. Yoon).
[1] These authors contributed equally to this work.

https://doi.org/10.1016/j.actamat.2017.09.068
1359-6454/

dissipated (P) as heat for a fixed voltage (V_a), simply because $P = V_a^2/R$, where R is resistance. In contrast, at fixed current, the power increases as $P = I^2R$, where I is current. This can generate thermal runaway in the heater, as the power supply tries to maintain a constant current. Maintaining constant power input with increasing resistance requires simultaneously increasing voltage and decreasing current. In many cases, formation of metal oxides can significantly increase the contact resistance at the NW junctions, reducing performance and ultimately causing irreversible degradation of the metal NWs.

For this reason, proper selections of materials and fabrication methods should be explored to overcome the oxidation issue of metal NWs. Here, we fabricated nickel (Ni)-electroplated fibers (NiEFs) using electrospinning followed by electroplating. Ni is slowly oxidized at room temperature. Accordingly, Ni has been actively used in the corrosion-resistive paints, coins, *etc.* The inherent corrosion resistance of Ni facilitated its outstanding performance as TCFs and THs, where both low R_s value of 0.73 Ω sq^{-1} with $T_r = 93\%$ and high heating temperature of 300 °C at 2.0 V were revealed. In addition, satisfactory mechanical properties were also demonstrated through bending and stretching tests, wherein the NiEFs were repeatedly bent over 2000 cycles and stretched up to 300% without electrical degradation.

2. Experimental method

2.1. Materials

The materials used to prepare solutions for electrospinning and nickel (Ni) electroplating, namely, polyacrylonitrile (PAN, $M_w = 150$ kDa), *N*,*N*-dimethylformamide (DMF, 99.8%), nickel (II) sulfamate tetrahydrate ($Ni(SO_3NH_2)_2{\cdot}4H_2O$, 98%), boric acid ($H_3BO_3$, 99.97%), sodium hydroxide solution (NaOH, 1.0 M), and formaldehyde (35%), were purchased from Sigma-Aldrich (USA). Ni frames, used as the substrates for the electrospun nanofibers (NFs), and pieces of Ni foil, used as the anodes for electroplating, were purchased from Wellcos Corporation (Republic of Korea) and Sigma-Aldrich (USA), respectively. Note that for the copper (Cu) electroplating process, the materials employed in Ref. [24] were used, including sulfuric acid (H_2SO_4, 99%, Matsunoen Chemical, Japan), hydrochloric acid (HCl, 37%, Sigma-Aldrich, USA), copper (II) sulfate ($CuSO_4$, 99%, Sigma-Aldrich, USA), formaldehyde (CH_2O, 37% Sigma-Aldrich, USA), and deionized (DI) water. For bending and stretching tests, Eco-flex was purchased from Smooth-On (Ecoflex 00-20, USA), which is comprised of platinum-catalyzed silicone polymer.

2.2. Prefabrication of polyacrylonitrile nanofibers

An 8 wt% yellow PAN solution formed using PAN and DMF as the solute and solvent, respectively, was used in electrospinning. As illustrated in Fig. 1(a), the PAN solution was supplied to an 18-gauge needle (Nordson EFD, USA) by a syringe pump (Legato 100, KD Scientific Inc., USA) at a flow rate, $Q_{es} = 200$ μl h^{-1}. A DC voltage, $V_{es} = 6.5$ kV was applied to the needle using a DC power supply (EP20P2, Glassman High Voltage Inc., USA). The PAN jet at the needle exit evolved, as in a typical electrospinning process, into PAN NFs, which were deposited and suspended on the Ni frame, as shown in Fig. 1(b). The distance between the needle and the Ni frame was fixed at 12 cm and the room temperature and humidity were also fixed during the experiments. The deposition (or electrospinning) time, t_{es}, was varied from 5 to 120 s to obtain NF mats with different transparencies. The frame-type substrate was used to obtain free-standing NFs. Note that the density and uniformity of the electrospun NFs can vary as the collector parameters are changed (e.g. size, distance-to-needle, temperature, shape, *etc.*) [25–28], which were not considered in the present work.

2.3. Fabrication of Ni- and Cu/Ni-electroplated fibers

The Ni electroplating solution was prepared by blending 80 g of $Ni(SO_3NH_2)_2{\cdot}4H_2O$, 6 g of H_3BO_3, and 200 mL of DI water [29]. The pH of the solution was adjusted to 4.5 by adding NaOH and then blending until the solution was homogeneous. The Cu electroplating solution was prepared using the process reported in our previous work [24]. Prior to the electroplating process, the free-standing PAN NFs were seeded with platinum (Pt) by sputtering (MSP-1S, Vacuum Device Inc., Japan). This allowed the non-conducting PAN NFs to be electroplated smoothly. Next, Ni-electroplated fibers (NiEFs) were formed as follows. First, the PAN NFs (suspended on the Ni frame) and a piece of Ni foil were immersed into the electroplating solution to be used as the cathode and anode, respectively (see Sec. 2.1.). Next, a current with the current density of 0.22 A cm^{-2}, which was based on the total area of the Ni frame [4 × 4 cm^2, cf. Fig. 1(b)], was transferred using a power supply (SPS-1820, GW Instek, Taiwan) for 60 s, as shown in Fig. 1(c) and Movie S1. The distance between the Ni frame and foil was 2 cm. Then, the plated sample was rinsed with 10% formaldehyde (diluted in DI water) and DI water for 10 min and 5 s, respectively. Finally, the rinsed sample was dried in a nitrogen atmosphere for a few minutes to prevent oxidation. This yielded NiEFs suspended on the Ni frame, as shown in Fig. 1(d). For the fabrication of the Cu/Ni-electroplated fibers (CuNiEFs), prior to the Ni electroplating process, Cu electroplating was performed on the PAN NFs by applying a voltage of 3 V for 10 s. The Cu-electroplated wires (CuEWs) were

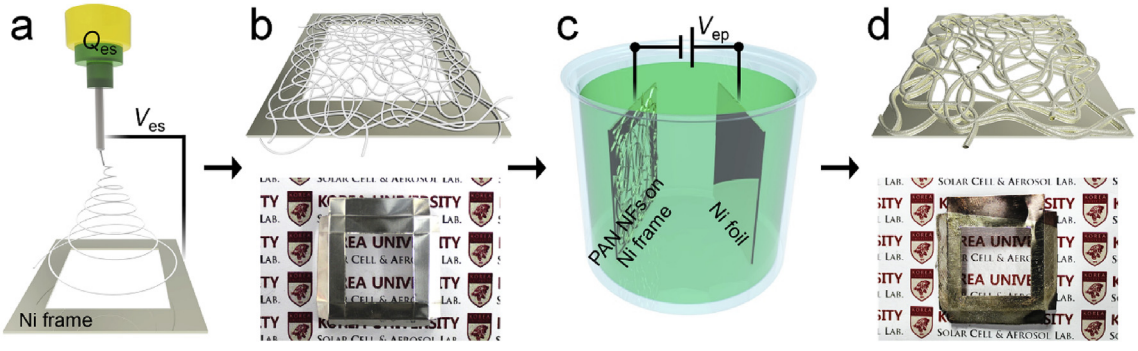

Fig. 1. Schematic of the NiEF fabrication process. (a) Electrospinning process, (b) free-standing electrospun PAN NFs collected on Ni frame ($t_{es} = 30$ s), (c) Ni electroplating process, and (d) NiEFs formed on Ni frame.

then rinsed and dried and subjected to Ni electroplating. The Ni electroplating for the CuNiEFs was conducted with a current density of 0.22 A cm^{-2} for 45 s.

Supplementary video related to this article can be found at https://doi.org/10.1016/j.actamat.2017.09.068.

2.4. Characterization

Scanning electron microscopy (SEM) was conducted using a field-emission SEM system with an energy-dispersive X-ray spectroscopy attachment (FE-SEM/EDX, Quanta 250 FEG, FEI). The average diameters of NiEFs were determined by measuring the diameters of 100 fibers in SEM images. The crystal structures and elemental compositions of the NiEFs were analyzed using X-ray diffraction (XRD) analysis (SmartLab, Rigaku) and X-ray photoelectron spectroscopy (XPS, X-tool, ULVAC-PHI), respectively. The transmittances (T_r) and sheet resistances (R_s) of NiEF samples were evaluated using an ultraviolet–visible spectrophotometry system (Optizen POP, Mecasys) and sheet resistance meter (FPP-400, Dasol Eng), respectively. Note that the 4-point probe method with the *dual*-configuration procedure was used to measure R_s values, where the distance between the pins was 1.59 mm. The reported values of R_s in each case are the average values of 30 points from 3 NiEF samples. The reported values of T_r (measured at $\lambda = 550$ nm) in each case are the average values of the same 3 NiEF samples that were previously used for the R_s measurements. Only one of the results for T_r is plotted to show T_r spectra. The NiEFs were transferred onto heat-resistant glass (D263) for the transmittance measurements (see photographs in Fig. 2). The heating experiments were conducted by applying voltage to the samples using a power supply (SPS-1820, GW Instek, Taiwan). Temperature was measured using a thermocouple and data recorder (MV1000, Yokogawa). Transmission electron microscopy (TEM) analysis of the CuNiEFs was performed using a TEM system (JEM 2100F, JEOL Inc.). The sample for the TEM analysis was prepared using a dual-beam focused ion beam (FIB) system (LVRA3 XMH, TESCAN).

3. Results and discussion

Fig. 2 shows photographs, SEM images, and elemental maps of the nickel (Ni)-electroplated fibers (NiEFs) formed using different electrospinning times (t_{es}). As mentioned previously, the as-fabricated NiEFs (see Fig. 1(d)) were transferred onto heat-resistant glass substrates before performing the heating tests. Thus, most characterizations were performed on these glass-based samples. The photographs in Fig. 2 clearly show transparent and translucent silver-colored NiEFs, which were obtained for low and high t_{es} values, respectively. The transmittance (T_r) values of the NiEFs formed at short electrospinning times, $t_{es} = 5$ and 30 s, were 93% and 83%, respectively, whereas those of the samples produced using long electrospinning times, $t_{es} = 60$ and 120 s, were 64% and 26%, respectively (see Table 1). Even though the diameters of the NiEFs (D_{avg}) were in the 3.71–4.75 μm range (Table 1), the open distances between the fibers, which were of the order of tens of microns, resulted in the high T_r values [24]. Note that the total transmittance of a material consists of its parallel and diffuse transmittances and that the parallel transmittance was measured in the present study [30].

Table 1
T_r ($\lambda = 550$ nm) and R_s values of NiEFs.

Case	Experimental result			Percolation model		
t_{es} (s)	D_{avg} (μm)	T_r (%)	R_s (Ω sq^{-1})	R	p	b
5	4.75	93	0.73	1.452	0.8017	0.0185
30	3.85	83	0.49	1.114	0.9296	0.0362
60	3.77	64	0.30	1.027	0.9834	0.0727
120	3.71	26	0.07	–		

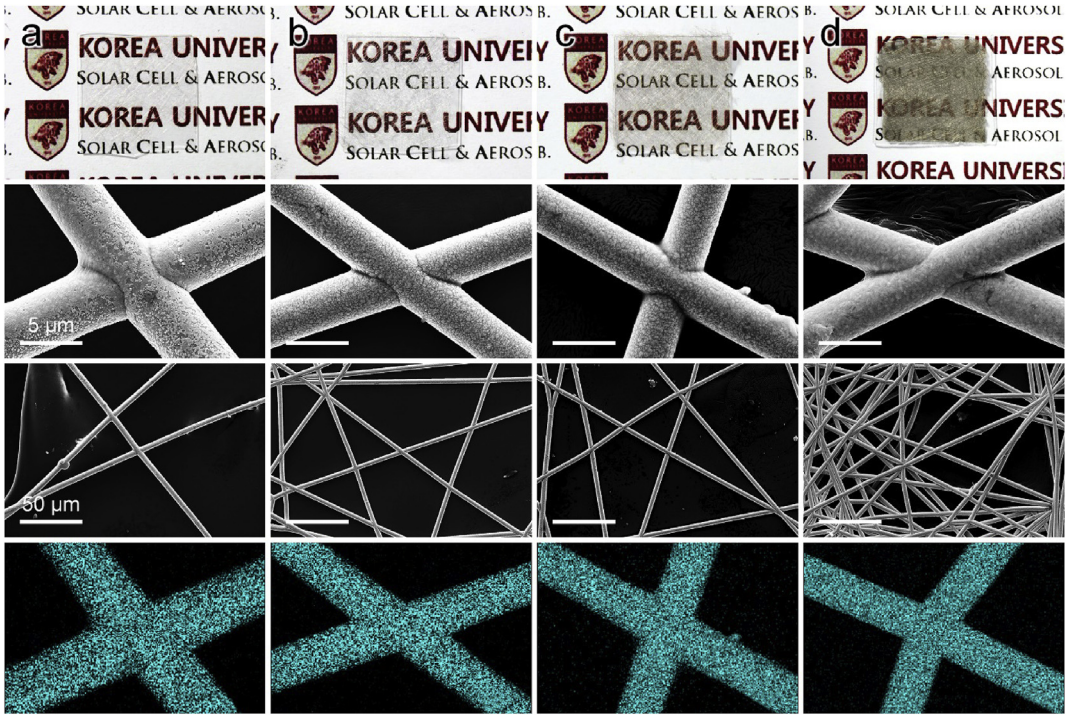

Fig. 2. Photographs, SEM images, and elemental maps of NiEFs formed with different t_{es}: (a) $t_{es} = 5$ s, (b) $t_{es} = 30$ s, (c) $t_{es} = 60$ s, and (d) $t_{es} = 120$ s. The samples for the photographs and SEM images were placed on glass substrates and pieces of carbon tape, respectively. Inset scale bars at each row are identical. Sky-blue dots in the elemental maps represent elemental Ni. (For interpretation of the references to colour in this figure legend, the reader is referred to the web version of this article.)

Regardless of the t_{es} value, the NiEFs exhibited smoothly-plated surfaces, with the fiber junctions being complete metallic bonds, as can be seen from the SEM images in Fig. 2. The smooth surfaces can be attributed to the fact that the NiEFs did not undergo oxidation during the fabrication process (see Sec. 2.3). In contrast, oxidized NiEFs, which were prepared by forcing oxidation, exhibited highly rough surfaces, as shown in Fig. 3 [29]. Ni does not undergo oxidation readily even at high temperatures or high oxygen pressures [31,32] and is therefore widely used as an industrial material in extreme environments.

Elemental maps (Fig. 2) and the XRD and XPS spectra (Fig. 4) confirmed that the NiEFs were composed of high-purity Ni without Ni_xO_x inclusions. Three main peaks can be seen in the XRD profile (Fig. 4(a)) at $2\theta = 44.6°$, 51.9°, and 76.5°; these correspond to the (111), (200), and (220) planes, respectively, of pure Ni (JCPDS No. 87-0712). The XPS spectrum (Fig. 4(b)) also contains Ni $2p_{3/2}$ and Ni $2p_{1/2}$ peaks, which are located at 852.6 and 869.9 eV, respectively, as well as satellite peaks; these are related to metallic Ni [33].

Both the presence of high-purity Ni and the complete bonding of the fibers at their junctions (see SEM images in Fig. 2) resulted in low electrical contact resistance [24]. Thus, the samples exhibited very low sheet resistance (R_s) values and high T_r values, as shown in Fig. 5(a) and Table 1. The R_s value decreased from 0.73 to 0.07 Ω sq^{-1} as t_{es} was increased from 5 to 120 s; accordingly, the T_r value decreased from 93% to 26%. This performance of the NiEFs is comparable to that of copper (Cu)-electroplated wires (CuEWs), which were recently reported to exhibit the lowest R_s values ever recorded, as well as high T_r [24]. Even though NiEFs synthesized in this work revealed a slightly poorer performance in comparison to that of CuEWs, NiEFs are more corrosion resistant than CuEWs. In addition, we emphasize that the properties of the NiEFs are superior to the corresponding properties of the majority of previously reported transparent conductive electrodes (TCEs, cf. Fig. 5(a)), including those made of Cu nanofibers (CuNFs) [13], silver nanowires (AgNWs) [34], gold (Au) NFs (AuNFs) [11], graphene [3], poly (3, 4-ethylenedioxythiophene) polystyrene sulfonate (PEDOT:PSS) [14], and single-walled carbon nanotubes (SWNTs) [35]. Note also the fact that the T_r of NiEFs remained unchanged for the wavelengths (λ) in the 400–800 nm range (Fig. 5(b)), which makes them attractive as a photoelectrochemical material for solar cells and photocatalytic water-splitting devices.

Next, the heating performance of the NiEFs as a thin transparent heater (TH) was examined, as illustrated in Fig. 5(c) and (d). Only the sample formed with $t_{es} = 5$ s was used for both the heating test and the cycling test, as it revealed the highest T_r value of 93%. Fig. 5(c) shows the heating temperature (T) of the NiEFs as a function of the applied voltage (V_a). T increased from 16.2 to 373 °C as V_a was increased from 0 to 2.0 V. The NiEFs started to degrade at 2.0 V and eventually broke after 150 s. This indicated that there is a threshold V_a that lies between 1.5 and 2.0 V, below which the NiEFs exhibit reversible heating characteristics, and above which, they degrade. It should be emphasized that the $T = 280$ °C of the NiEFs at $V_a = 1.5$ V exceeds those reported for heaters based on nanomaterials such an AgNWs, CNTs, and graphene, which exhibited T values in the 48–160 °C [14–18], 77–160 °C [6,7,9,36], and 100–206 °C [4,5,37] ranges, respectively. Furthermore, the NiEFs maintained their heating capability and did not degrade after 20 cycles ($V_a = 1$ V), as shown in Fig. 5(d). This suggests that NiEFs could be well-suited for use in various industrial applications.

We also performed bending and stretching tests to evaluate the flexibility and stretchability of NiEF mats, as shown in Fig. 6. The free-standing NiEFs ($t_{es} = 5$ s) were transferred onto flexible polyethylene terephthalate [PET, see Fig. 6(a)] and Eco-flex films for the bending and stretching tests, respectively. During the tests, the NiEFs not only retained their conductivity over 2000 cycles (red in Fig. 6(b)) but also revealed a remarkable stretchability, which was as high as 300% (blue in Fig. 6(b)). Even though a significant degradation was observed after stretching by 250% during the

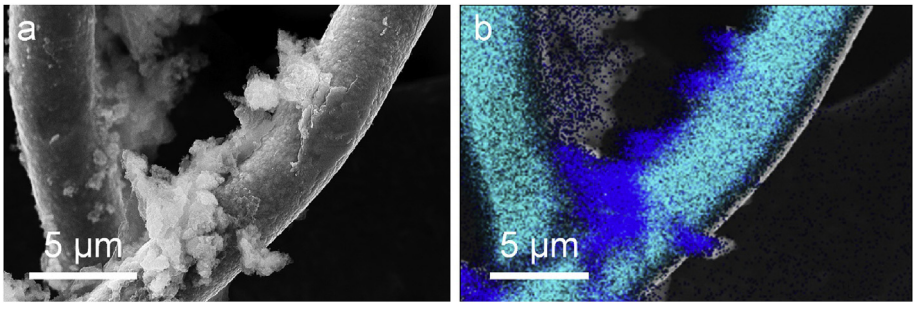

Fig. 3. (a) SEM image and (b) the elemental map of oxidized NiEFs. Sky-blue and deep-blue dots in the elemental map represent elemental Ni and O, respectively. (For interpretation of the references to colour in this figure legend, the reader is referred to the web version of this article.)

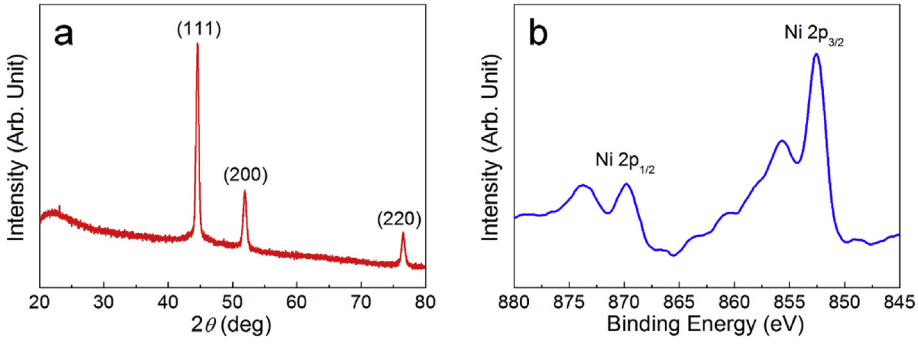

Fig. 4. (a) XRD and (b) high-resolution XPS spectra of NiEFs.

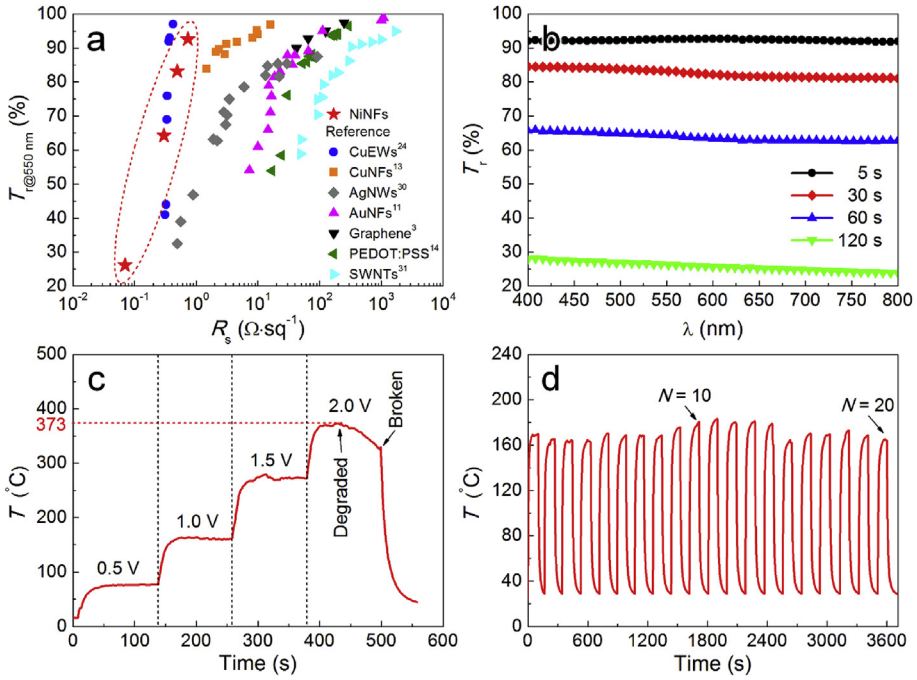

Fig. 5. (a) T_r and R_s of NiEFs as functions of t_{es}. The t_{es} values were t_{es} = 5, 30, 60, and 120 s from top to bottom red-stars. T_r of CuEWs, CuNFs, AgNWs, AuNFs, graphene, PEDOT:PSS, and SWNTs are shown for comparison. (b) T_r spectra of NiEFs formed with different t_{es} values. (c) Results of heating and (d) cycling tests of NiEFs (t_{es} = 5 s). (For interpretation of the references to colour in this figure legend, the reader is referred to the web version of this article.)

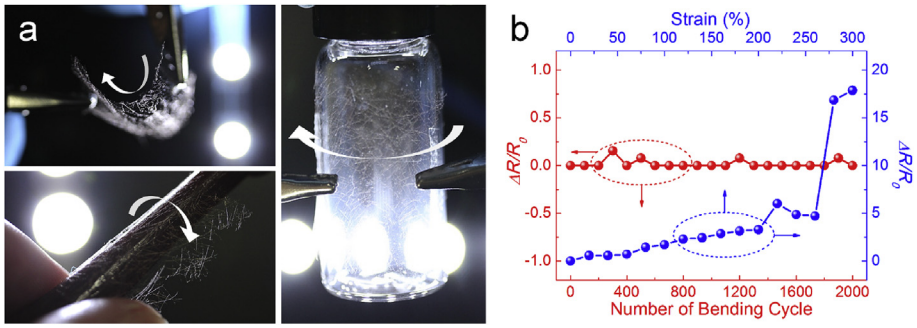

Fig. 6. (a) Photographs of LED operation using free-standing NiEFs (t_{es} = 5 s) that were transferred onto a PET substrate. (b) Effect of bending and uniaxial stretching of NiEFs (t_{es} = 5 s).

stretching test, these results are comparable to those of the previous studies [11,13]. Thus, the mechanical stability and durability of NiEFs, as well as their ability to provide uniform heating (see Fig. 7) highlight their suitability for use in a wide range of applications.

Fig. 8 shows cross-sectional TEM images and elemental maps of Cu/Ni-electroplated fibers (CuNiEFs). As mentioned above, the sample for the TEM analysis was prepared by the FIB milling method (see Fig. S1) [38]. By sequentially electroplating Cu and Ni on PAN NFs (see Sec. 2.3), perfectly core-shell-structured CuNiEFs could be obtained, as shown in Fig. 8(b)–(e). The elemental maps confirm that the CuNiEFs consisted of high-purity Ni shells and Cu cores. The thicknesses of the Ni and Cu layers could be adjusted by varying the electroplating parameters (see Sec. 2.3).

To demonstrate high corrosion resistance of NiEFs, long-time heating tests under the 60% relative humidity (for rapid oxidation) were conducted as shown in Figs. S2 and S3. The same V_a = 0.5 V was applied to the CuEWs, NiEFs, and CuNiEFs, which resulted in the temperature range of 80–100 °C. Note that the values of D_{avg} of the three samples were in the 3–5 μm range. After 1800 s heating, the CuEWs were distinctly degraded (Fig. S2) and Cu_xO_x crystals were clearly visible on their surface in SEM images (Fig. S3(b)). The O content of the CuEWs after heating (measured by EDX) was 5 wt%. In contrast to the CuEWs, the NiEFs and the CuNiEFs not only exhibited no degradation for 2000 s heating but also revealed no signs of oxidation (Fig. S2, S3(c), S3(d), S3(e)).

To theoretically analyze the behavior of such materials [34], we recently proposed a percolation model based on the classical percolation theory [24,39,40]. It should be emphasized that the new percolation model was used to describe one-dimensional conductive materials using the renormalization group technique used in the percolation theory. The percolation model involves two primary parameters: the probability of bond occupancy, p, and the shading factor, b. These two parameters are correlated to the t_{es} (see Fig. 2) and the D_{avg} of the individual NiEFs (see Table 1), respectively. Based on the calculation methods proposed in Ref. [24], we determined the p and b values of the NiEFs as functions of t_{es} (see Table 1 and Supporting Information for details). Note that this percolation model is strictly applicable only to single-projected

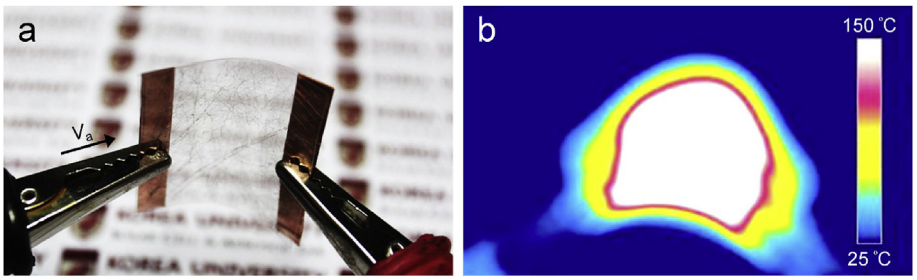

Fig. 7. (a) Photograph and (b) infrared image of free-standing NiEFs at V_a = 1 V (t_{es} = 5 s).

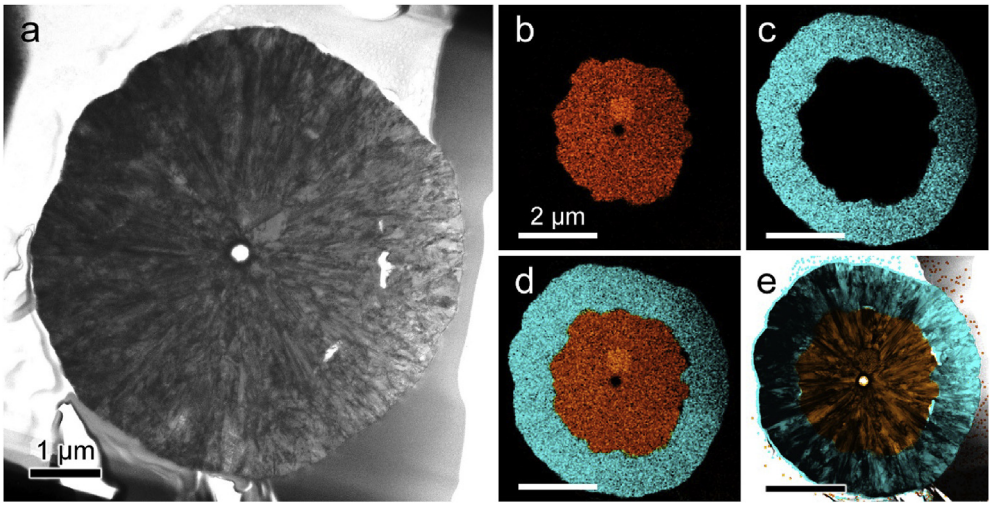

Fig. 8. (a) Cross-sectional TEM image and (b, c, d) elemental maps of FIB-sectioned CuNiEF sample: (b) only core, (c) only shell, and (d) core-shell structure. (e) Combined TEM image of (a) and (d). Orange and sky-blue dots in the elemental maps represent elemental Cu and Ni, respectively. (For interpretation of the references to colour in this figure legend, the reader is referred to the web version of this article.)

structures (see Fig. 2(a)–(c)) because it is based on two-dimensional bond lattices without overlapping. Thus, this percolation model was unsuitable for the sample corresponding to t_{es} = 120 s, which exhibited a multi-layered overlapping structure (see Fig. 1(d)). As t_{es} was increased, the p and b values increased. The increased number of the deposited NFs and the corresponding NF conglutination resulted in the increase in the values of p and b (see Fig. 2 and Table 1) [24]. Note that the value of D_{avg} of the NiEFs decreased gradually as t_{es} increased because the total mass of electroplated Ni onto the nanofibers was constant owing to the fact that the electroplating time and the current density of all cases were, respectively, fixed at 60 s and at 0.22 A cm^{-2} (see Sect. 2.3).

4. Conclusions

Although different transparent conducting films (TCFs) with reasonably high flexibilities, conductivities, and transmittances have been previously reported, they have found limited use because not all the above-mentioned characteristics were present simultaneously. In the present study, by combining electrospinning and electroplating, we successfully formed nickel (Ni)-electroplated fibers (NiEFs) and copper (Cu)/Ni-eletroplated fibers (CuNiEFs), which are not subject to these limitations. The present NiEFs formed a percolative network with perfect metallic bonding of the individual fibers. They exhibited reversible bendability over 2000 cycles, high stretchability of up to 300%, an exceedingly low sheet resistance (R_s) of 0.73 Ω sq^{-1}, and, when used as resistive heaters, heating temperature greater than 300 °C (at 2.0 V). At the same time, they also exhibited excellent transmittance (T_r) of 93%. Electrospun polymer nanofibers (NFs) were electroplated with Ni to obtain flexible and transparent high-purity Ni electrodes, which formed a percolative network. The fact that the NiEFs exhibited remarkably high electrical conductivity, as well as a high optical transmittance, can be attributed to the so-called self-junctioning phenomenon during electroplating and the percolative network derived from the nonwoven polymer NFs used. Furthermore, when these NiEFs are used as the electrodes in transparent heaters (THs) and TCFs, the inherent corrosion resistance of Ni can significantly improve the long-term device performance. In addition, we sequentially plated polymer NFs with Cu and Ni to obtain perfectly core-shell-structured Cu/Ni fibers. Given these extraordinary characteristics, as well as simple and inexpensive manufacturing, and thus a commercially viable and scalable nature of the proposed method, these nanomaterials hold great promise as advanced TCFs and THs.

Acknowledgements

This research was supported by the Technology Development Program to Solve Climate Changes of the National Research Foundation (NRF) funded by the Ministry of Science, ICT and Future Planning (NRF-2016M1A2A2936760), NRF-2013M3A6B1078879, and NRF-2017R1A2B4005639.

Appendix A. Supplementary data

Supplementary data related to this article can be found at https://doi.org/10.1016/j.actamat.2017.09.068.

References

[1] G. Eda, G. Fanchini, M. Chhowalla, Large-area ultrathin films of reduced graphene oxide as a transparent and flexible electronic material, Nat. Nanotechnol. 3 (5) (2008) 270–274.

[2] K.S. Kim, Y. Zhao, H. Jang, S.Y. Lee, J.M. Kim, K.S. Kim, J.-H. Ahn, P. Kim, J.-Y. Choi, B.H. Hong, Large-scale pattern growth of graphene films for stretchable transparent electrodes, Nat 457 (7230) (2009) 706–710.

[3] S. Bae, H. Kim, Y. Lee, X. Xu, J.-S. Park, Y. Zheng, J. Balakrishnan, T. Lei, H.R. Kim, Y.I. Song, Roll-to-roll production of 30-inch graphene films for transparent electrodes, Nat. Nanotechnol. 5 (8) (2010) 574–578.

[4] J. Kang, H. Kim, K.S. Kim, S.-K. Lee, S. Bae, J.-H. Ahn, Y.-J. Kim, J.-B. Choi, B.H. Hong, High-performance graphene-based transparent flexible heaters, Nano Lett. 11 (12) (2011) 5154–5158.

[5] J.J. Bae, S.C. Lim, G.H. Han, Y.W. Jo, D.L. Doung, E.S. Kim, S.J. Chae, T.Q. Huy, N. Van Luan, Y.H. Lee, Heat dissipation of transparent graphene defoggers, Adv. Funct. Mater. 22 (22) (2012) 4819–4826.

[6] Y.H. Yoon, J.W. Song, D. Kim, J. Kim, J.K. Park, S.K. Oh, C.S. Han, Transparent film heater using single-walled carbon nanotubes, Adv. Mater. 19 (23) (2007) 4284–4287.

[7] D. Kim, H.-C. Lee, J.Y. Woo, C.-S. Han, Thermal behavior of transparent film heaters made of single-walled carbon nanotubes, J. Phys. Chem. C 114 (13) (2010) 5817–5821.

[8] D.S. Hecht, L. Hu, G. Irvin, Emerging transparent electrodes based on thin films of carbon nanotubes, graphene, and metallic nanostructures, Adv. Mater. 23 (13) (2011) 1482–1513.

[9] D. Jung, D. Kim, K.H. Lee, L.J. Overzet, G.S. Lee, Transparent film heaters using multi-walled carbon nanotube sheets, Sens. Actuators A 199 (2013) 176–180.

[10] A.R. Rathmell, B.J. Wiley, The synthesis and coating of long, thin copper nanowires to make flexible, transparent conducting films on plastic substrates, Adv. Mater. 23 (41) (2011) 4798–4803.

[11] S. Soltanian, R. Rahmanian, B. Gholamkhass, N.M. Kiasari, F. Ko, P. Servati, Highly stretchable, sparse, metallized nanofiber webs as thin, transferrable transparent conductors, Adv. Energy Mater. 3 (10) (2013) 1332–1337.

[12] P.-C. Hsu, S. Wang, H. Wu, V.K. Narasimhan, D. Kong, H.R. Lee, Y. Cui, Performance enhancement of metal nanowire transparent conducting electrodes by mesoscale metal wires, Nat. Commun. 4 (2013).

[13] H. Wu, D. Kong, Z. Ruan, P.-C. Hsu, S. Wang, Z. Yu, T.J. Carney, L. Hu, S. Fan, Y. Cui, A transparent electrode based on a metal nanotrough network, Nat. Nanotechnol. 8 (6) (2013) 421–425.

[14] T. Kim, Y.W. Kim, H.S. Lee, H. Kim, W.S. Yang, K.S. Suh, Uniformly interconnected silver-nanowire networks for transparent film heaters, Adv. Funct. Mater. 23 (10) (2013) 1250–1255.

[15] R. Gupta, K. Rao, K. Srivastava, A. Kumar, S. Kiruthika, G.U. Kulkarni, Spray coating of crack templates for the fabrication of transparent conductors and heaters on flat and curved surfaces, ACS Appl. Mater. Interfaces 6 (16) (2014) 13688–13696.

[16] P.-C. Hsu, X. Liu, C. Liu, X. Xie, H.R. Lee, A.J. Welch, T. Zhao, Y. Cui, Personal thermal management by metallic nanowire-coated textile, Nano Lett. 15 (1) (2014) 365–371.

[17] S. Sorel, D. Bellet, J.N. Coleman, Relationship between material properties and transparent heater performance for both bulk-like and percolative nanostructured networks, ACS Nano 8 (5) (2014) 4805–4814.

[18] S. Hong, H. Lee, J. Lee, J. Kwon, S. Han, Y.D. Suh, H. Cho, J. Shin, J. Yeo, S.H. Ko, Highly stretchable and transparent metal nanowire heater for wearable electronics applications, Adv. Mater. 27 (32) (2015) 4744–4751.

[19] L. Li, Z. Yu, W. Hu, C.h. Chang, Q. Chen, Q. Pei, Efficient flexible phosphorescent polymer light-emitting diodes based on silver nanowire-polymer composite electrode, Adv. Mater. 23 (46) (2011) 5563–5567.

[20] Y.H. Kim, J. Lee, S. Hofmann, M.C. Gather, L. Müller-Meskamp, K. Leo, Achieving high efficiency and improved stability in ITO-free transparent organic light-emitting diodes with conductive polymer electrodes, Adv. Funct. Mater. 23 (30) (2013) 3763–3769.

[21] Z. Yu, L. Li, Q. Zhang, W. Hu, Q. Pei, Silver nanowire-polymer composite electrodes for efficient polymer solar cells, Adv. Mater. 23 (38) (2011) 4453–4457.

[22] D. Bryant, P. Greenwood, J. Troughton, M. Wijdekop, M. Carnie, M. Davies, K. Wojciechowski, H.J. Snaith, T. Watson, D. Worsley, A transparent conductive adhesive laminate electrode for high-efficiency organic-inorganic lead halide perovskite solar cells, Adv. Mater. 26 (44) (2014) 7499–7504.

[23] K. Im, K. Cho, J. Kim, S. Kim, Transparent heaters based on solution-processed indium tin oxide nanoparticles, Thin Solid Films 518 (14) (2010) 3960–3963.

[24] S. An, H.S. Jo, D.Y. Kim, H.J. Lee, B.K. Ju, S.S. Al-Deyab, J.H. Ahn, Y. Qin, M.T. Swihart, A.L. Yarin, Self-junctioned copper nanofiber transparent flexible conducting film via electrospinning and electroplating, Adv. Mater. 28 (33) (2016) 7149–7154.

[25] C.H. Kim, Y.H. Jung, H.Y. Kim, D.R. Lee, N. Dharmaraj, K.E. Choi, Effect of collector temperature on the porous structure of electrospun fibers, Macromol. Res. 14 (1) (2006) 59–65.

[26] D. Zhang, J. Chang, Patterning of electrospun fibers using electroconductive templates, Adv. Mater. 19 (21) (2007) 3664–3667.

[27] O. Yördem, M. Papila, Y.Z. Menceloğlu, Effects of electrospinning parameters on polyacrylonitrile nanofiber diameter: an investigation by response surface methodology, Mater. Des. 29 (1) (2008) 34–44.

[28] C. Vaquette, J.J. Cooper-White, Increasing electrospun scaffold pore size with tailored collectors for improved cell penetration, Acta Biomater. 7 (6) (2011) 2544–2557.

[29] S. Sinha-Ray, Y. Zhang, A.L. Yarin, Thorny devil nanotextured fibers: the way to cooling rates on the order of 1 kW/cm^2, Langmuir 27 (1) (2011) 215–226.

[30] K. Manabe, S. Nishizawa, K.-H. Kyung, S. Shiratori, Optical phenomena and antifrosting property on biomimetics slippery fluid-infused antireflective films via layer-by-layer comparison with superhydrophobic and antireflective films, ACS Appl. Mater. Interfaces 6 (16) (2014) 13985–13993.

[31] S. Mrowec, Z. Grzesik, Oxidation of nickel and transport properties of nickel oxide, J. Phys. Chem. Solids 65 (10) (2004) 1651–1657.

[32] S. Han, H.-Y. Chen, C.-C. Chen, T.-N. Yuan, H.C. Shih, Characterization of Ni nanowires after annealing, Mater. Lett. 61 (4) (2007) 1105–1108.

[33] A.P. Grosvenor, M.C. Biesinger, R.S.C. Smart, N.S. McIntyre, New interpretations of XPS spectra of nickel metal and oxides, Surf. Sci. 600 (9) (2006) 1771–1779.

[34] S. De, P.J. King, P.E. Lyons, U. Khan, J.N. Coleman, Size effects and the problem with percolation in nanostructured transparent conductors, ACS Nano 4 (12) (2010) 7064–7072.

[35] V. Scardaci, R. Coull, J.N. Coleman, Very thin transparent, conductive carbon nanotube films on flexible substrates, Appl. Phys. Lett. 97 (2) (2010) 023114.

[36] H.-S. Jang, S.K. Jeon, S.H. Nahm, The manufacture of a transparent film heater by spinning multi-walled carbon nanotubes, Carbon 49 (1) (2011) 111–116.

[37] D. Sui, Y. Huang, L. Huang, J. Liang, Y. Ma, Y. Chen, Flexible and transparent electrothermal film heaters based on graphene materials, Small 7 (22) (2011) 3186–3192.

[38] L. Giannuzzi, F. Stevie, A review of focused ion beam milling techniques for TEM specimen preparation, Micron 30 (3) (1999) 197–204.

[39] D. Stauffer, Scaling theory of percolation clusters, Phys. Rep. 54 (1) (1979) 1–74.

[40] D. Stauffer, A. Aharony, Introduction to Percolation Theory, CRC Press, Boca Raton, 1994.